Journal of Micromechanics and Microengineering

Copper foil-type vibration-based electromagnetic energy harvester

To cite this article: Farid Khan *et al* 2010 *J. Micromech. Microeng.* **20** 125006

IOP PUBLISHING JOURNAL OF MICROMECHANICS AND MICROENGINEERING

J. Micromech. Microeng. **20** (2010) 125006 (11pp) doi:10.1088/0960-1317/20/12/125006

Copper foil-type vibration-based electromagnetic energy harvester

Farid Khan[1], **Farrokh Sassani**[1] **and Boris Stoeber**[1,2]

[1] Department of Mechanical Engineering, The University of British Columbia, Vancouver, BC V6T 1Z4, Canada

[2] Department of Electrical and Computer Engineering, The University of British Columbia, Vancouver, BC V6T 1Z4, Canada

E-mail: farid72@interchange.ubc.ca

Received 29 July 2010, in final form 16 September 2010
Published 9 November 2010
Online at stacks.iop.org/JMM/20/125006

Abstract

This paper presents the modeling, simulation, fabrication and experimental results of a vibration-based electromagnetic power generator (EMPG). A novel, low-cost, one-mask technique is used to fabricate the planar coils and the planar spring. This fabrication technique can provide an alternative for processes such as lithographie galvanoformung abformung (LIGA) or SU-8 molding and MEMS electroplating. Commercially available copper foils of 20 μm and 350 μm thicknesses are used for the planar coils and planar spring, respectively. The design with planar coils on either side of the magnets provides enhanced power generation for the same footprint of the device. The harvester's overall volume is 1 cm^3. Excitation of the EMPG, at the fundamental frequency of 371 Hz, base acceleration of 13.5 g and base amplitude of 24.4 μm, yields an open circuit voltage of 60.1 mV, as well as 46.3 mV load voltage and 10.7 μW power for a 100 Ω load resistance. At a matching impedance of 7.5 Ω the device produced a maximum power of 23.56 μW and a power density of 23.56 μW cm^{-3}. The simulations based on the analytical model of the device show good agreement with the experimental results.

(Some figures in this article are in colour only in the electronic version)

1. Introduction

Wireless sensor nodes have a wide range of applications from condition monitoring of rotary machines, such as electric motors and compressors, to tire pressure monitoring systems (TPMS) in automobiles. One of the most challenging problems for wireless sensor nodes is the power source [1, 2]. Batteries have a limited life and their use in wireless sensor nodes may restrict the application of such devices in embedded and harsh environments. Harvesting energy from the ambient will have a significant impact on the field of wireless sensors. Converting ambient mechanical vibration into electrical energy for wireless sensor nodes with vibration-based micro power generators (MPGs) is suitable for applications such as non-destructive health monitoring of structures and machines. In industrial machines, such as electric motors, generators, compressors, reciprocating engines or turbines, vibration levels for a frequency range of 0–5000 Hz vary from 0.5 to 15 g peak acceleration [3], whereas the vibration levels for some production machines, such as lathes and drilling presses, and for household appliances typically range from 30 to 200 Hz and vary from 0.01 to 1.1 g peak acceleration [4]. The goal is to develop vibration-based power generators suitable for harvesting energy from these commonly available vibration levels to power wireless transmitters and sensors. The power levels of vibration-based energy harvesters tend to be low; however, with the rapid advancement in ultra-low power (ULP) MEMS sensors and microelectronics, the power need is on a decline to few μW. The power requirements of commercially available ULP sensors depend on the type (pressure, temperature or acceleration) and model of the sensor. For operation, ULP acceleration sensors need more power (21.6–324 μW for supply current levels of 1.7–2.5 μA) in comparison to pressure sensors (1.8–8.4 μW for supply current levels of 1–4 μA) and temperature sensors (1.89–37.8 μW for supply current levels of 2.1–2.7 μA).

The overall power consumption of these ULP sensors ranges from 1.8 to 324 μW for supply current levels of 1–180 μA [5]. Due to these ULP needs, energy harvesting has the potential for integrating into these sensors to provide unlimited maintenance-free operation. Wireless sensor power needs are typically a few mW [2], which is relatively high and a major portion of the power is required for RF transmission. The current MEMS-scale energy harvesting techniques are not developed far enough to completely eliminate the battery from wireless sensor nodes; however, upon subjecting the device output voltage to an ultra-low voltage (ULV) and ULP rectifier, and the resulting dc voltage to an ULV dc–dc step-up converter, these harvesters can be usefully integrated to supplement the power provided by the battery and increase its life span.

Several vibration-based power generators, based on piezoelectric [6], electrostatic [7] and electromagnetic [8] transduction, have been demonstrated. Out of these, electromagnetic power generators (EMPGs) have the advantages of low output impedance and high output current levels [9]. Vibration-based electromagnetic energy harvesters typically consist of a permanent magnet, a coil and a suspension spring. Electrical energy is generated when the coil experiences a change in the magnetic flux as a result of a relative motion between the magnet and the coil and an emf is generated across its ends according to the Faraday law of electromagnetic induction. There are two well-known architectures used for EMPGs to achieve this energy transduction. In one architecture of EMPGs, the magnet is mounted on a suspension spring and the coil is stationary, whereas in the other type the magnet is fixed and the coil rides on a suspension spring. However, the former is preferred since the magnet acts as the inertial mass and this has the advantage of lowering the resonant frequency and enhancing the device's power generation, since power generation has direct dependence on the inertial mass [10]. For both EMPG architectures, different fabrication approaches to produce the coils and the suspension springs have been reported in the literature.

1.1. Moving magnet EMPGs

This type of EMPG mostly consists of a bulk permanent magnet bonded to a microfabricated planar spring, and a coil, which is either a microfabricated planar coil or a wound coil. Wang *et al* [11] have reported a moving magnet-type MPG, comprised of a NdFeB magnet, a two-layer planar copper coil on a glass substrate and a planar copper spring fabricated on a double-side thermally oxidized silicon wafer. The planar spring is fabricated by selective etching of SiO_2 with buffered hydrofluoric acid (BHF), sputtering of Cr/Cu as a seed layer, molding and electroplating of copper, and backside wet etching of silicon and SiO_2. Each layer of the coil is produced by molding and electroplating of copper. A 150 nm Cr/Cu seed layer is sputtered for this purpose. A cured, grinded and polished polyimide layer is used as insulation between the two copper coils. A 2 mm × 2 mm × 1 mm NdFeB magnet is attached to the platform of the planar spring, which is then bonded onto the substrate containing the copper coils to form a MPG. The reported maximum 60 mV peak-to-peak open circuit voltage was generated at 121.3 Hz for 1.5 g base acceleration. A silicon MPG for wearable micro devices reported in [12] consists of a planar spring and a magnet which moves within a central recess of the substrate carrying the coil. The nickel–iron (Ni-Fe) spring is fabricated on a silicon wafer with the following process steps: application of nitride by low pressure chemical vapor deposition (LPCVD), backside patterning of nitride, and etching of silicon with potassium hydroxide (KOH) to obtain a supporting 30 μm silicon membrane, deposition of a Ti/Cu seed layer on the front side, molding and electroplating of a 20 μm thick Ni-Fe layer, and finally the etching of the backside silicon membrane and nitride by reactive ion etching (RIE) releasing the suspension spring. The planar copper coil is fabricated on the second silicon wafer using backside patterning of the nitride layer, silicon etching with KOH to achieve the supporting silicon membrane, sputtering and patterning of an aluminum layer on the front side, plasma-enhanced chemical vapor deposition (PECVD) of oxide as an insulation layer, sputter deposition of Ti/Cu as a seed layer, followed by molding and electroplating of 100 μm thick copper. As a last step, a backside silicon and nitride etch by RIE produces the central recess for the movement of the magnet. After mounting the NdFeB magnet on the center plate of the spring wafer, it is adhesive bonded to the coil wafer to form a 6 mm × 6 mm × 1 mm MPG. The MPG generated 1.4 μW when excited at 100 Hz and 50 μm base amplitude. Pan *et al* [13] reported the development of a two-wafer MPG, in which a sputtered iron–platinum (Fe-Pt) magnet on a spiral planar spring is used instead of a bulk magnet. In their device the silicon spiral spring is fabricated by bulk micromachining with a double-sided polished silicon wafer. The fabrication involves selective deep reactive ion etching (DRIE) to define the spiral, depositing a SiO_2/Si_3Ni_4 layer, backside selective etching of silicon by KOH to form a spiral spring and then sputtering of the magnetic Fe-Pt film. A planar copper coil is made with a 4-mask process that needs a buffer layer coating, copper seed layer sputtering, molding and electroplating of routing copper, insulator polyimide layer coating and mold electroplating of copper. The two wafers are then joined by a low temperature bonding process to form a 0.45 cm^3 device. The authors reported a 40 mV voltage amplitude and 100 μW power generation at the excitation frequency of 60 Hz. A membrane-type EMPG, containing a 127 μm thick kapton membrane to support NdFeB magnets, that moves within a recess provided in a silicon wafer (wafer 1), and within a printed circuit board (PCB) frame (wafer 2) has been reported by Serre *et al* [14]. The recess is produced by bulk micro-machining. A 52 turn, 15 μm thick electroplated planar copper coil, fabricated on a recessed silicon wafer is bonded to the recessed PCB wafer. The kapton membrane is glued to the backside of the PCB wafer to form the complete device. The response of their fabricated device is nonlinear. Under resonant condition at 5.1 μm base amplitude it produced a maximum power of 50 μW at matched load and a maximum voltage of 180 mV at a resistance load of 100 k Ω.

A combined electromagnetic and piezoelectric generator for harvesting energy from a computer keyboard is reported in [15]. The electromagnetic element of the device consists of a NdFeB magnet, a rubber cushion spring and a micro-machined bi-layer planar aluminum coil. Five masks are used to fabricate the bi-layer aluminum planar coil on a thin lead zirconate titanate (PZT) plate. The fabrication comprises 0.5 μm thick parylene deposition and patterning with RIE to open the contact pads for the PZT electrode, sputter deposition of 0.6 μm thick aluminum and patterning for the first spiral coil, deposition and patterning of 0.5 μm parylene as an insulation layer, sputtering and patterning of 0.6 μm thick aluminum for the second spiral coil, and lastly deposition of 0.5 μm parylene as a passivation layer. For electromagnetic conversion the authors reported a maximum of 1.15 μW with a 35 Ω load for a typing speed of 40 words per minute. The development of a wound copper coil harvester with NdFeB magnets and a tungsten proof mass on the tip of a laser etched beryllium copper (BeCu) cantilever beam is reported in [16]. The detailed fabrication of the 2800 turn stationary coil and 50 μm thick BeCu beam is not reported. The 150 mm^3 generator produced a power of 58 μW at 52 Hz and 0.6 m s^{-2} acceleration, and successfully powered an RF accelerometer sensor. An AA battery size power generator for wireless applications, which is composed of a hand wound coil and a spiral planar spring to support the magnet, is reported in [17]. The spiral spring is fabricated by laser micromachining as well as by SU-8 molding and electroplating. A magnet is attached to the central platform of the spring and an inner housing, having a recess for the movement of the magnet, is bonded on either side of the spring. A wire is wound on the inner housing to form a coil for the power generator. It has been shown that when two such power generators are integrated with a power management circuit (rectifiers and a capacitor) and packaged into an AA battery size container, it produced 1.6V dc when subjected to vibration and charged for less than 1 min.

1.2. Moving coil EMPGs

In a moving coil EMPG the coil moves relative to a fixed permanent magnet with the help of a suspension spring to generate the electrical power. A proof mass has to be used to tune the resonant frequency and enhance the power generation. Sari *et al* [18] developed a moving coil-type EMPG for wideband environmental vibrations that consists of an array of coil embedded cantilever beams and a fixed magnet. The EMPG is fabricated with a 5-mask process. The fabrication steps involved are the thermal growth of 1 μm thick SiO_2, deposition and patterning of 1 μm thick parylene with RIE, sputtering and patterning of Ti/Au as a coil material, deposition and patterning of 1 μm thick parylene as an isolation layer, metal deposition for electrical routing, deposition of 13 μm thick parylene to define cantilevers, backside silicon etching by DRIE, and finally the sacrificial oxide etching by BHF resulting in the release of the beams. With an array of 35 beams and excitation at 1 μm base amplitude the reported device produced 10 mV voltage and 0.4 μW power over a bandwidth of 800 Hz (4.2–5 kHz). Kulkarni *et al* [19] developed an MPG consisting of four fixed NdFeB magnets and a planar copper coil fabricated on a silicon paddle. The fabrication of the planar coil and the silicon paddle comprised of chemical vapor deposition (CVD) of 0.5 μm thick oxide, sputtering and patterning of a 2 μm thick copper layer for electrical routing, deposition and patterning of 1.8 μm thick polyamide, molding and electroplating of the copper as coil, and DRIE with a patterned photoresist to form the silicon paddle, beam and frame. Two NdFeB magnets are assembled in a polymethylmethacrylate (PMMA) chip that is fabricated by conventional milling. The silicon chip and two such PMMA chips are then bonded together to produce a 0.1 cm^3 MPG. At the resonant frequency of 9.84 kHz and for 9.8 m s^{-2} acceleration the MPG has shown to generate a maximum power of 23 nW at a load of 52.7 Ω. An EMPG developed with standard silicon micromachining is reported in [20]. The EMPG consists of four fixed NdFeB magnets, a cantilevered paddle and a wound coil. The silicon paddle, frame and cantilever beam are fabricated by DRIE. A V groove in the cantilever beam (to channel the copper wire from the wound coil to the pads) is produced by selective etch of SiO_2/Si_3Ni_4 and KOH etch of the silicon, and the aluminum pads are made by metallization and selective etching. Two magnets are positioned within the mechanically machined recess in the capping PMMA chip. One of such PMMA chips is then bonded onto either side of the silicon chip to form a 100 mm^3 device. The device generated 122 nW of power for 0.4 g input acceleration at 9.5 kHz. An EMPG that consists of a hand wound coil attached to an etched stainless steel beam, which moves between two fixed NdFeB magnets is reported in [21]. The device has a natural frequency of 322 Hz and generated a maximum power of 37 μW at a base amplitude of 13 μm. Soliman *et al* [22] report a wideband energy harvester consisting of four fixed magnets, a seismic mass and a wound coil supported by an aluminum cantilever beam. The 1 cm^2 wound coil has 22 turns and is made out of 160 μm thick copper wire. The details of the fabrication of the beam are not reported. A sliding stopper is used to restrict the motion of the beam to transform the harvester from a linear oscillator to a piecewise-linear oscillator. It has been shown that with this transformation a broad bandwidth is obtained in the vicinity of the natural frequency.

In EMPGs, the fabrication of micro-coils, accurate mounting of the high flux density permanent magnets, and the spring that supports the magnets or coil are challenging steps. Multi-mask microfabrication processes are typically used to produce planar coils and springs for EMPGs adding complexity to fabrication and contributing to high fabrication cost of such devices. Most of the previously reported approaches use silicon-based multi-mask or complex fabrication methods to develop planar coils and planar springs. Applications to low cost wireless sensors require a simple and cost effective fabrication process with a small number of masks and fabrication steps, using low cost materials and eliminating expensive process steps.

This paper reports the fabrication of vibration-based EMPG in which the planar coil and the planar spring are fabricated by a novel, low cost, one mask process. The planar

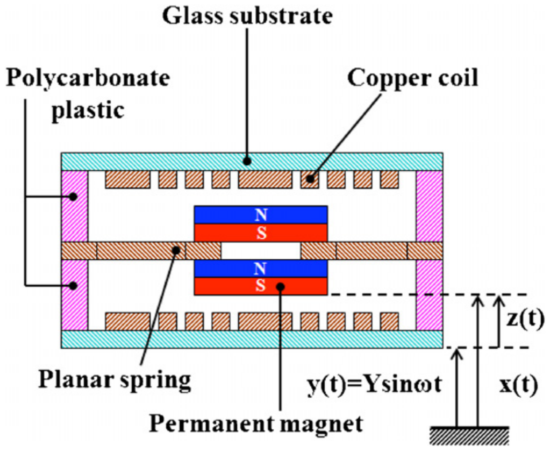

Figure 1. Cross-sectional view of the developed EMPG.

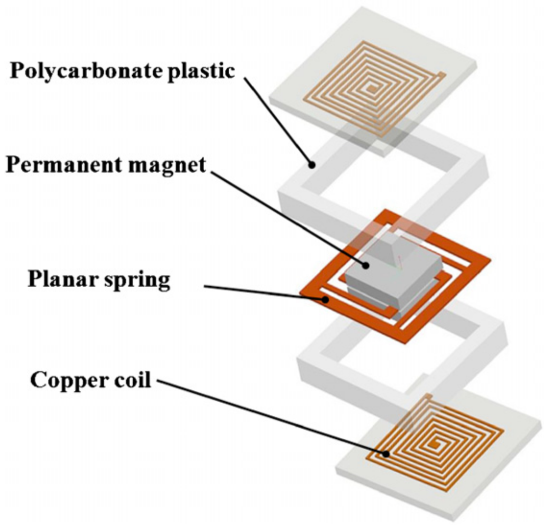

Figure 2. Exploded view of the EMPG.

copper coils and the planar spring to support the motion of the permanent magnets have been fabricated from commercially available copper foils. Two identical coils are used, one on either side of the magnets in order to enhance the power generation for the same footprint of the EMPG. The detailed modeling and simulation for a device configuration in which a magnet is vibrating on top of a coil is performed and is found in good agreement with the experimental results. The equivalent electrical circuit model is used to extract the electrical damping ratio for load power computation.

2. Design and modeling

The EMPG presented in this paper consists of two NdFeB magnets (K & J Magnetics Inc. Jamison, PA, USA) mounted on a planar copper spring as shown in figure 1. Planar copper micro-coils, fabricated on a glass substrate are placed on either side of the magnet assembly. The magnets and the micro-coils are held apart by 2 mm thick polycarbonate plastic spacers (Sheffield Plastics Inc. Sheffield, MA, USA). Figure 2 illustrates the exploded view of the device.

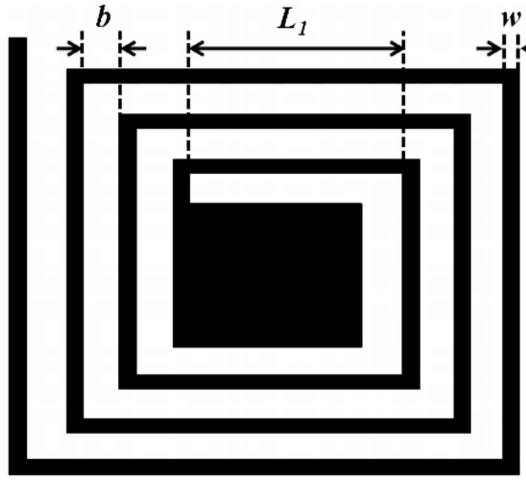

Figure 3. Square spiral planar coil.

By modeling the EMPG shown in figure 1 as spring-mass-damper system with base excitation, the amplitude of the relative displacement

$$Z = \frac{(Y\omega^2)}{\omega_n^2\sqrt{\left[1-\left(\frac{\omega}{\omega_n}\right)^2\right]^2+\left[2\zeta_T\left(\frac{\omega}{\omega_n}\right)\right]^2}} \tag{1}$$

and the amplitude of the relative velocity

$$U = \frac{A\omega}{\omega_n^2\sqrt{\left[1-\left(\frac{\omega}{\omega_n}\right)^2\right]^2+\left[2\zeta_T\left(\frac{\omega}{\omega_n}\right)\right]^2}} \tag{2}$$

between the magnets and housing of the device are determined in terms of the frequency of excitation ω, the natural frequency ω_n, the base amplitude of vibration Y, the base acceleration $A = \omega^2 Y$ and the total damping ratio ζ_T.

The induced open-circuit voltage in a single coil of the device is approximated according to Faraday's law of electromagnetic induction [23, 24] as

$$V_G = -U\frac{\mathrm{d}B_z}{\mathrm{d}z}S, \tag{3}$$

where B_z is the normal magnetic flux density and S is the sum of the areas S_i of the individual coil turns.

For a square spiral planar coil, figure 3, with the length L_1 of the side of the first turn, line width w and spacing b between the adjacent turns, S can be approximated as

$$S = \sum_{i=1}^{n} S_i \approx \sum_{i=1}^{n} L_i^2 \tag{4}$$

$$L_i = L_1 + 2(i-1)(w+b), \tag{5}$$

where L_i is one side length of a turn.

The magnetic flux density for a rectangular block magnet [25] along a line normal to its center

$$B_z = \frac{B_r}{\pi}\left\{\sin^{-1}\left[\frac{WD}{4\left[\left(\frac{W^2}{4}+z^2\right)\left(\frac{D^2}{4}+z^2\right)\right]^{1/2}}\right] - \sin^{-1}\left[\frac{WD}{4\left[\left(\frac{W^2}{4}+(z+T)^2\right)\left(\frac{D^2}{4}+(z+T)^2\right)\right]^{1/2}}\right]\right\} \tag{6}$$

depends on the remanent flux density B_r, the width of magnet W, the length of the magnet D, the thickness or the combined thickness of the two magnets T in our case and the distance from the magnets z.

For the analytical computations, $\frac{\mathrm{d}B_z}{\mathrm{d}z}$ is obtained by differentiating equation (6) with respect to z and then setting z equal to the gap between the magnet and a coil at rest.

The amplitude of the voltage

$$V_L = \left(\frac{R_L}{R_L + R_C}\right) S\frac{\mathrm{d}B_z}{\mathrm{d}z} \frac{A\omega}{\omega_n^2\sqrt{\left[1-\left(\frac{\omega}{\omega_n}\right)^2\right]^2 + \left[2\zeta_T\left(\frac{\omega}{\omega_n}\right)\right]^2}} \tag{7}$$

and the amplitude of the power

$$P_L = \frac{V_L^2}{2R_L} \tag{8}$$

delivered to the load depend on the load resistance R_L and the coil resistance R_C.

The maximum voltage

$$V_{L,1} = \left(\frac{R_L}{R_L + R_C}\right) S\frac{\mathrm{d}B_z}{\mathrm{d}z}\frac{A}{2\omega_n\zeta_T} \tag{9}$$

occurs at resonance.

The analytical model (equation (7)) predicts very good estimates for the EMPGs in which the planar coil is much smaller than the magnet and for small gaps between the coil and the magnet. However, it will slightly overestimate the EMPG performance if the outer edges of the coil face a smaller flux density than the maximum flux density given by equation (6).

The transformation factor G is an important parameter in inertial EMPGs. It describes the coupling between the mechanical and electrical energy domains and it therefore describes the energy conversion between the mechanical and the electrical domains. The open-circuit induced voltage across the coil

$$V_G = GU \tag{10}$$

is therefore expressed by the transformation factor, and the force

$$F_e = GI \tag{11}$$

acts on the magnet due to the current I flowing through the coil. Using equations (10) and (11), an inertial EMPG can be represented by the equivalent electrical circuit model shown in figure 4. In the mechanical domain m, b_m and k represent the inertial mass, mechanical damping coefficient and spring stiffness, respectively. By ignoring the coil self-inductance L_C that corresponds to a very small impedance at the frequencies of interest and combining the load and coil series resistances, the input impedance at the transformer element is expressed as

$$r_m = \frac{R_L + R_C}{G^2}. \tag{12}$$

In the equivalent electrical circuit in figure 4(*b*), the total damping coefficient of the EMPG $b_T = b_m + b_e$ includes the electrical damping coefficient

$$b_e = \frac{1}{r_m} = \frac{G^2}{R_L + R_C}. \tag{13}$$

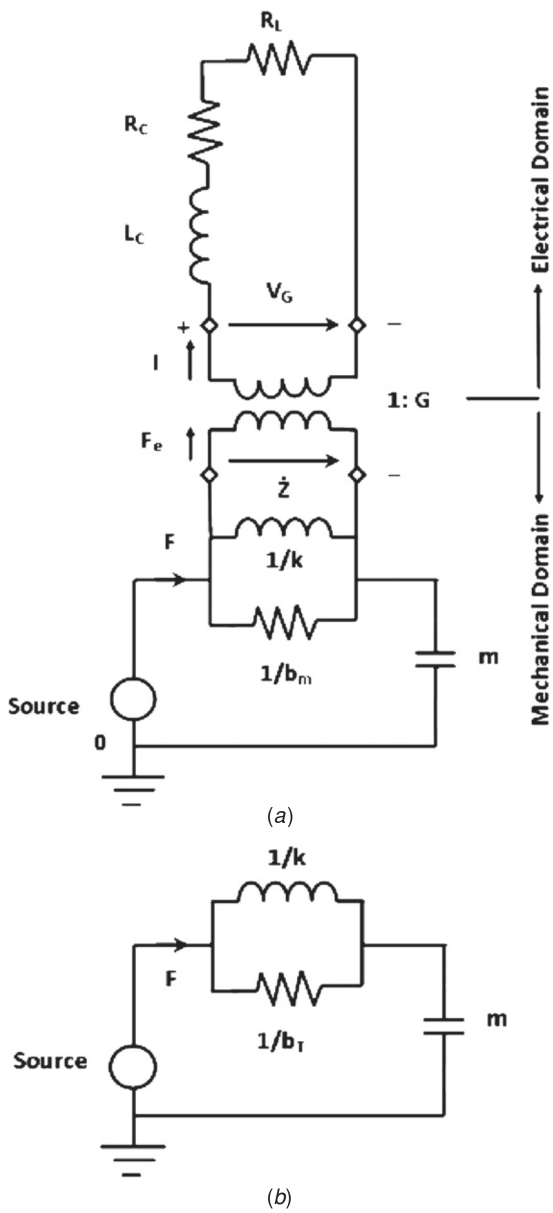

Figure 4. (*a*) Equivalent circuit model for an inertial EMPG, (*b*) equivalent circuit with the combined damping coefficient.

The transformation factor

$$G = S\frac{\mathrm{d}B_z}{\mathrm{d}z} \tag{14}$$

for our device configuration can be found from equations (3) and (10). The electrical damping coefficient b_e and critical damping coefficient b_c describe the electrical damping ratio ζ_e, and using equations (13) and (14) the electrical damping ratio of the device can be expressed as

$$\zeta_e = \frac{1}{2m\omega_n(R_L + R_C)} S^2 \left(\frac{\mathrm{d}B_z}{\mathrm{d}z}\right)^2. \tag{15}$$

Equations (8), (9) and (15) yield the load power at resonance

$$P_{L,1} = \left(\frac{R_L}{R_L + R_C}\right)\frac{m\zeta_e}{4\omega_n}\left(\frac{A}{\zeta_m + \zeta_e}\right)^2 \tag{16}$$

in terms of the electrical damping ratio ζ_e and the mechanical damping ratio ζ_m, where $\zeta_e + \zeta_m = \zeta_T$.

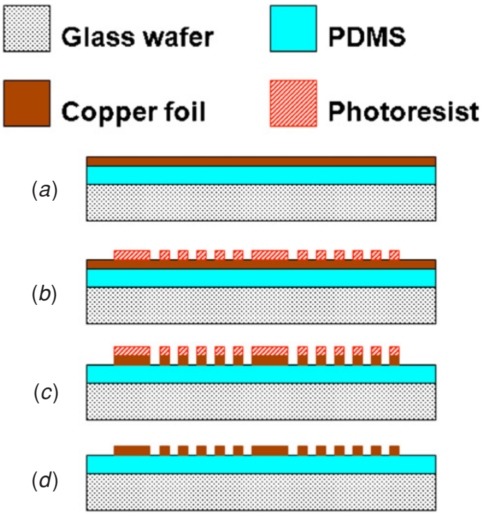

Figure 5. Fabrication steps of the copper micro-coil: (*a*) spin coat a PDMS layer on a glass wafer, and force bond a copper foil, (*b*) spin coat photoresist and perform photolithography, (*c*) copper etch using a dilute nitric acid solution, (*d*) strip off photoresist.

By eliminating the damping ratios ζ_e and ζ_m, equation (16) can be expressed in the form

$$P_{L,1} = \frac{G^2 S^2 m^2}{2} \frac{R_L}{[b_m(R_L + R_C) + G^2]^2}, \tag{17}$$

which is more suitable to derive the optimum power condition for impedance matching. Optimizing equation (17) with respect to R_L yields the condition for optimum power transfer to the load as

$$R_{L,\mathrm{opt}} = R_C + \frac{G^2}{b_m}. \tag{18}$$

In EMPGs with large transformation factor G and small mechanical damping coefficient b_m the second term on the right-hand side of equation (18) can be significant; however, for meso- and micro-scale EMPGs with planar coils, this term is negligible in comparison to the coil resistance R_C and can be ignored as will be shown for our device.

3. Fabrication of the prototype

The fabrication process of the planar copper coils is illustrated in figure 5. A 20 μm thick copper foil (Comet Metal Inc., Walton Hills, OH, USA) is bonded onto a glass substrate with polydimethylsiloxane (PDMS) (Dow Corning Corporation, Midland, MI, USA). PDMS (mixture of 10 parts elastomer base and 1 part elastomer curing agent) is spun on the glass substrate at 500 rpm for 10 s followed by 1000 rpm for 30 s. Then the copper foil is pressed onto the uncured PDMS layer, using a weight of 196 N on top of the copper foil at room temperature to provide a uniform pressure for bonding, figure 5(*a*). Cleanroom wipes are used between the dead weight and the substrate in order to prevent direct contact of the weight and the foil. After 1 h the weight is removed and the sample is put into an oven at 80 °C for 2 h in order to cure the PDMS, which results in bonding of the copper foil to the glass substrate. Photoresist SPR 220–7 (Rohm and Haas Company, Philadelphia, PA, USA) is then spun on, exposed with a mask aligner using a mask and is then developed, figure 5(*b*). The copper foil is etched with a dilute solution of nitric acid (80 ml HNO_3 and 160 ml H_2O) at room temperature for 10 min, figure 5(*c*). Finally, the photoresist is stripped off using acetone, figure 5(*d*). Microscopic images of a fabricated micro-coil are shown in figure 6.

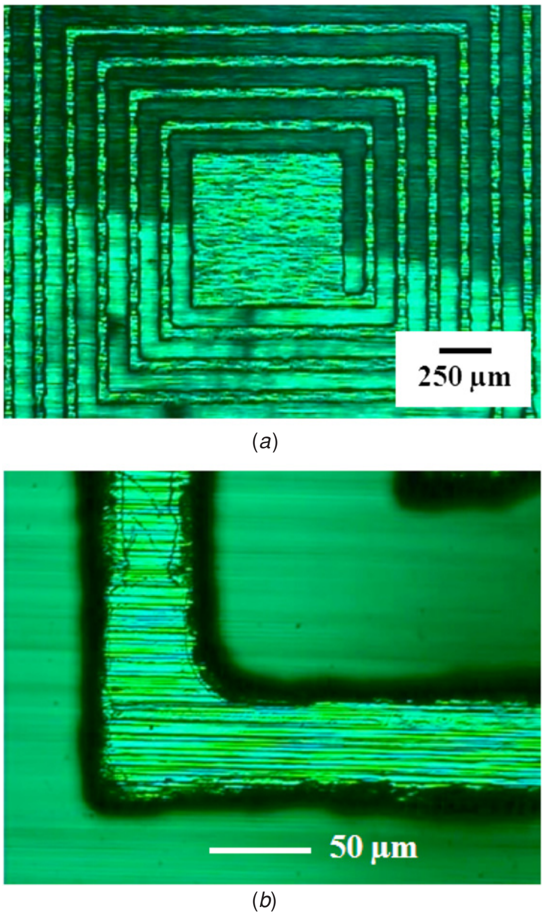

Figure 6. (*a*) Microscopic image of a copper micro-coil, (*b*) detailed view of a section of the coil.

The fabrication process of the planar copper spring used to support the permanent magnet is shown in figure 7. The process starts with spinning a sacrificial layer of the negative photoresist SU-8 2075 (MicroChem Corp., Newton, MA, USA) onto a silicon wafer, followed by force bonding of a 350 μm thick copper foil (Storm Copper Components Co., Decatur, TN, USA) to the wafer, figure 7(*a*). Again, the dead weight of 196 N is used for 1 h, to provide a uniform pressure to bond the copper foil to the wafer. The weight is removed and the wafer is then soft baked on a hot plate at 95 °C for 10 min. Photoresist SPR 220–7 is then spun on, exposed and developed, figure 7(*b*). The selective etching of the copper foil is then performed using a 50% dilute solution of nitric acid (80 ml HNO_3 and 80 ml H_2O) at room temperature for 15 min, figure 7(*c*). The fabricated structures are then separated from the wafer using SU-8 developer, figure 7(*d*). Finally the separated structures are cleaned with acetone to remove the photoresist, figure 7(*e*). Figure 8 shows the fabricated structures.

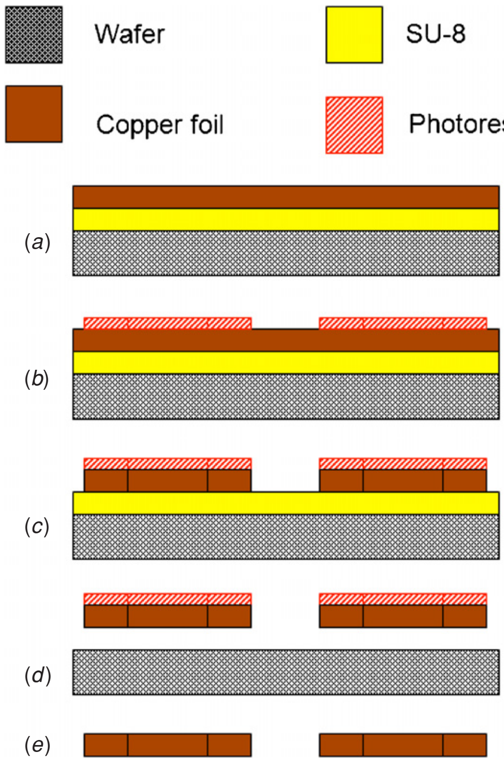

Figure 7. Fabrication steps of the planar spring: (*a*) spin cast photoresist SU-8 2075 and force bond a copper foil to the wafer, (*b*) spin coat photoresist SPR 220–7 followed by exposure and development, (*c*) copper etch in dilute nitric acid, (*d*) strip off SU-8 in developer solution, (*e*) strip off SPR 220–7 with acetone.

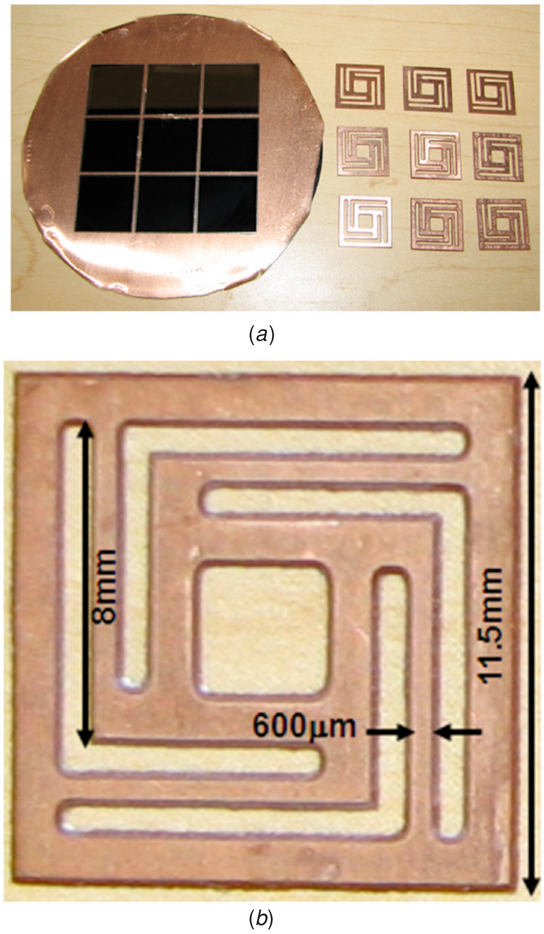

Figure 8. Photographs of batch fabricated planar springs: (*a*) processed copper foil on a silicon wafer with nine planar springs, (*b*) one of the planar springs.

The assembly of the EMPG is done under a stereo microscope (Olympus SZ61, Olympus Imaging America Inc., Center Valley, PA, USA). First, the two permanent magnets are mounted on the planar spring with the help of a specially designed jig, as shown in figures 9(*a*) and (*b*). No adhesive is used to bond the magnets to the copper spring, but rather the force of attraction between the magnets is exploited to tightly sandwich the planar spring between the magnets, figure 9(*c*). Two polycarbonate plastic spacers are then bonded on either side of the planar spring with epoxy; by doing so the sides of the planar spring are firmly sandwiched between the two spacers, figure 9(*d*). Finally, the glass substrates, containing the micro-coils are bonded to the spacers, using the same adhesive, as shown in figures 9(*e*) and (*f*). The dimensions and parameters of the assembled EMPG are listed in table 1.

4. Experimental setup and results

Figure 10 shows the schematic of the experimental setup used for the measurement of natural frequencies, vibration amplitude and voltage output from the EMPG. The laser head and vibrometer (Polytech Inc., Northbrook, IL, USA) are used for the measurement of the vibration of the mass (magnets) and the device housing. The voltage output signal from the device and the signal from the vibrometer are simultaneously read by the oscilloscope. The function generator and power amplifier control the frequency and vibration amplitude of the shaker (Type 4809, Bruel & Kjaer, Naerum, Denmark). A 7 cm thick Teflon spacer block is mounted onto the shaker table to safeguard the device from the ferromagnetic parts of the shaker. The EMPG and an accelerometer (MMA1200EG, Freescale Semiconductor, Austin, TX, USA) are bonded to the Teflon block by a double-sided adhesive tape.

Figure 11 shows the amplitude of the relative displacement between the magnets and a coil as a function of excitation frequency. The experimental data are obtained without the top coil in place; instead, a transparent glass piece is bonded to the top plastic spacer, such that the laser from the vibrometer could be focused on the top magnet. A 100 Ω load resistance is connected to the bottom coil and the EMPG is subjected to a frequency sweep from 200 to 800 Hz at $A = 13.5$ g base acceleration amplitude. The experimental results show the first three natural frequencies 371, 616 and 725 Hz, with the relative displacement between the magnets and the coils at these frequencies at 142.4, 52 and 38.6 μm, respectively. For simulation purposes the total damping ratio was calculated using the relationship

$$\zeta_T = \frac{Y}{2Z_{\max}} = \frac{A}{8\pi^2 f_1^2 Z_{\max}}, \tag{19}$$

where $Z_{\max}$ is the relative displacement between the magnets and the coil at the fundamental frequency f_1. At the resonant

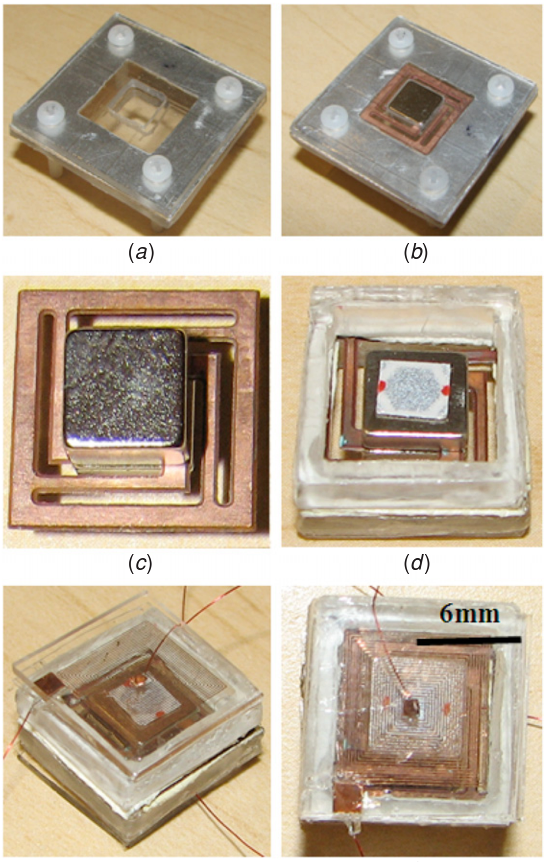

Figure 9. Photographic images of the prototype during various stages of assembly: (*a*) jig for mounting magnets onto planar spring, (*b*) magnets and planar spring in the jig, (*c*) magnets mounted onto the planar spring, (*d*) planar spring sandwiched between the plastic spacers, (*e*) glass substrates, containing the micro-coils bonded to the spacers, (*f*) top view of the assembled EMPG.

Table 1. Dimensions and parameters of the EMPG prototype.

Description	Value
Device size	12 mm × 12 mm × 7 mm
Magnet (NdFeB), B_r	1.2–1.32 T
Magnet dimensions	6 mm × 6 mm × 1.5 mm
Mass of each magnet	0.465 g
Coil size	8 mm × 8 mm
Gap between magnet and coil	500 μm
No of turns of coil	21
Resistance of coil	7.5 Ω
Spring beam length	8 mm
Spring beam thickness	350 μm
Spring beam width	600 μm

frequency of $f_1 = 371$ Hz equation (19) yields a total damping ratio $\zeta_T = 0.0857$.

The relative displacement given by equation (1) is also plotted in figure 11 using the measured fundamental natural frequency of 371 Hz and the measured damping ratio ζ_T. A modal analysis performed in COMSOL multiphysics® confirms that the fundamental resonant frequency of 371 Hz corresponds to the mode during which the magnets vibrate normal to the plane of the spring, whereas the two higher

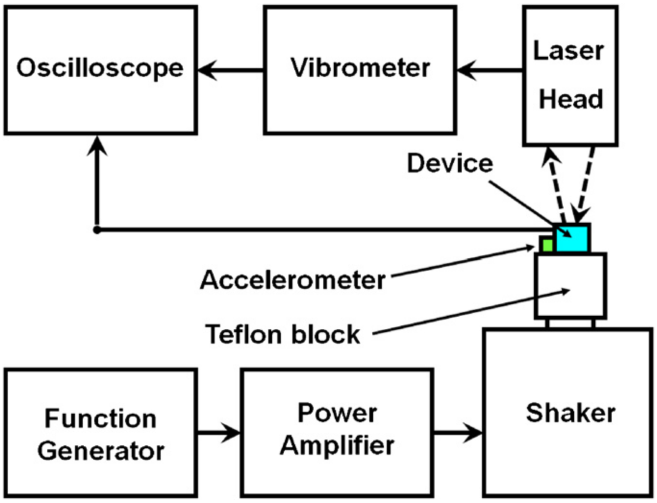

Figure 10. Schematic of the experimental setup.

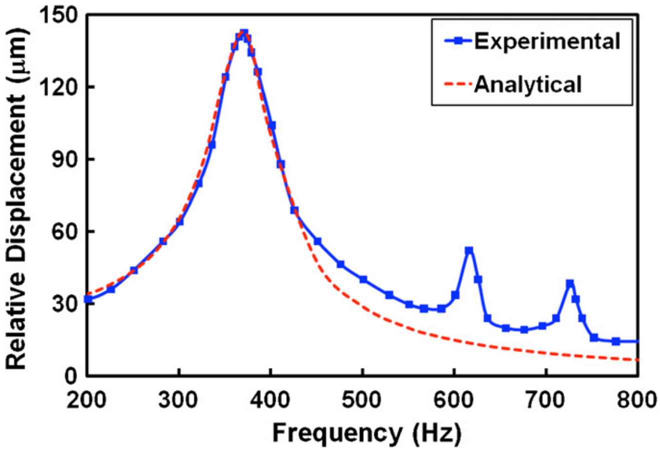

Figure 11. Relative displacement of the magnets versus input frequency at 13.5 g base acceleration amplitude.

resonant frequencies of 616 and 725 Hz correspond to the rotational modes where the magnets rotate about an axis parallel to the plane of the coil [26].

Open circuit potentials (OCP) of 31.9 and 28.2 mV are produced by the two coils when the EMPG is excited at the first resonance frequency of 371 Hz at 13.5 g. The difference in the output signals of the coils is postulated to be due to fabrication inaccuracies. A 100 Ω resistance is connected to each coil and voltage signals across the resistances are mathematically summed in the oscilloscope to obtain the combined load voltage generated by the EMPG.

Figure 12 shows the load voltage amplitude measured experimentally and computed based on the model equation (7) using $\mathrm{d}B/\mathrm{d}z = 124.8\ \mathrm{T\ m^{-1}}$. When the EMPG is subjected to a frequency sweep from 200 to 800 Hz at 13.5 g acceleration amplitude, a maximum voltage of 46.3 mV is generated at the load at the fundamental frequency of 371 Hz. The voltage delivered at the second and third modes are 16.8 and 17.9 mV, respectively.

The power delivered to the 100 Ω load resistance as a function of frequency is plotted in figure 13. The measured

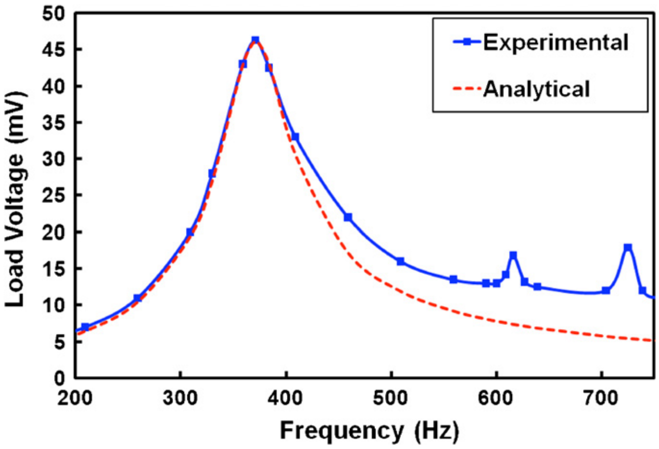

Figure 12. Load voltage for a 100 Ω load versus frequency at 13.5 g base excitation.

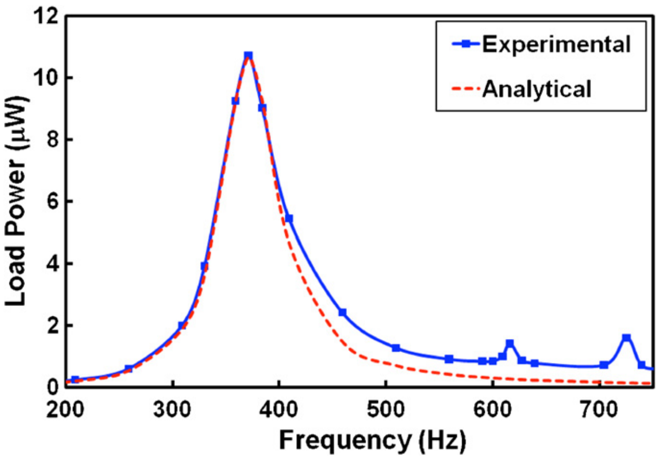

Figure 13. Power delivered to the load versus frequency for a 100 Ω load resistance and 13.5 g base excitation.

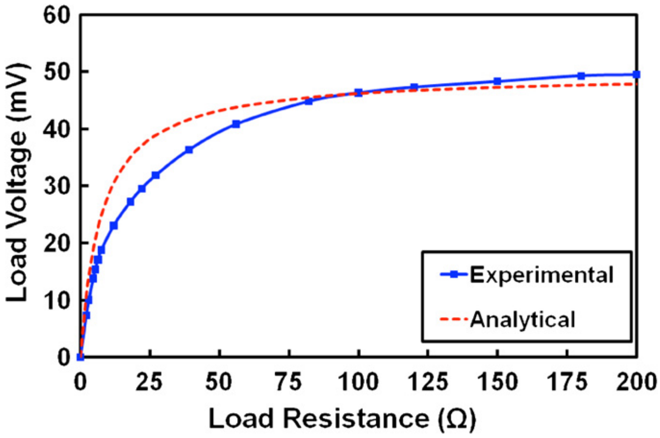

Figure 14. Load voltage versus load resistance at 371 Hz and 24.4 μm (13.5 g) base excitation.

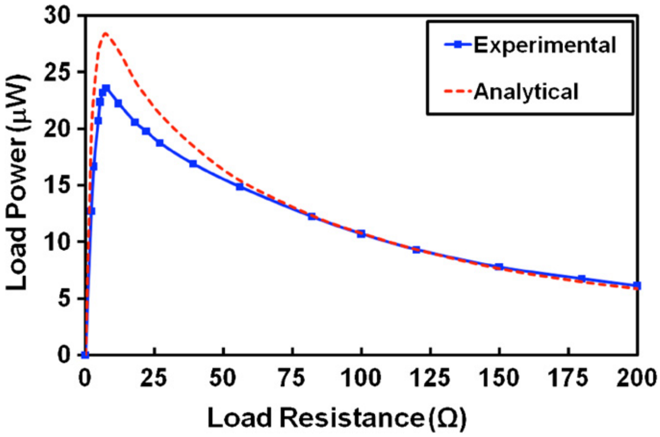

Figure 15. Power versus load resistance at 371 Hz and 24.4 μm (13.5 g) base excitation.

voltage across the 100 Ω load resistance is used to compute the power delivered to the load resistance whereas the analytical values are obtained from equation (8). The experimental data indicate that both coils are capable of producing a combined power of 10.7, 1.4 and 1.6 μW at 371, 616 and 725 Hz, respectively. Good agreement was found between the analytical and experimental results for displacement, voltage and power around the fundamental frequency. However, at relatively higher frequencies (beyond 390 Hz) a deviation between the curves appears, which is due to the presence of higher resonant modes and indicates that the device is no longer following the assumed single degree of freedom analytical model.

Figures 14 and 15 show the load voltage and power versus resistive load. Different load resistances were connected to the EMPG and it was excited at the first mode resonance frequency of 371 Hz at 13.5 g acceleration. The simulated load voltage and power are found using equations (9) and (16), respectively. For simulation purposes the electrical damping ratio ζ_e is calculated with equation (15) for different load resistances. Knowing the electrical damping ratio at 100 Ω, the mechanical damping ratio ζ_m is extracted from the experimentally computed total damping ratio at 100 Ω. Figures 14 and 15 indicate that the larger the load resistor, the larger is the measured voltage and the smaller is the through current. The maximum voltage measured was 49.5 mV for the maximum load resistance 200 Ω in our experiments and the maximum power obtained from the EMPG was about 23.56 μW for a load resistance of about 7.5 Ω that is identical to the resistance of the coils. The term G^2/b_m in the expression for the optimum load (equation (18)) is only 0.014 Ω for our device, which is small in comparison to the coil resistance of 7.5 Ω and can be ignored as mentioned earlier. Based on the harvester overall volume of 1 cm^3 and operating at the matching impedance the optimum power density of the device is 23.56 μW cm^{-3}.

The voltage levels generated by the developed EMPG are in the mV range (46.3 to 60.1 mV); however, due to the low optimum load impedance of the device, which is only 7.5 Ω, relatively high current levels are expected. The EMPG has sufficient power producing capability to operate the majority of the ULP sensors mentioned in the introduction. However, for the relatively high supply voltage (1.8 to 2.7 V) requirements of these sensors, the low output ac voltage signal of the EMPG will need to be conditioned with an

Table 2. Summary of vibration-based EMPGs.

Type		Materials: Spring	Materials: Coil	V_{load} (mV_{pk})	R_{load} (Ω)	R_{coil} (Ω)	F (Hz)	P_{max} (μW)	Volume (cm^3)	Y (μm)	A (g_{pk})	Power density ($\mu W\ cm^{-3}$)	References
Moving magnet	Planar coil	Cu	Cu	30	–	–	121.3	–	0.004	–	1.5	–	[11]
		Ni-Fe	Cu	–	–	2	100	1.44	0.036	50	2[a]	40	[12]
		Si	Cu	40	–	–	60	100	0.45		–	222	[13]
		Kapton	Cu	180	100k	100	340	50	1.35	5	2.3[a]	40	[14]
		Rubber	Al	–	35	–	–	1.15	–	–	–	–	[15]
		Cu	Cu	9[b]	33	33	55	0.61	0.13	–	1.52	4.7	[30]
		PDMS	Cu	84.3	100	10.1	111	61.5	2.25	–	3	27.33	[5]
		Acrylic	Cu	3.2	0.8	0.8	948	3.2	–	14	50.7[a]	–	[27]
		–	Cu	9	50	50	40–80	0.4	2.27	–	1.9	0.148	[28]
		Cu	Cu	46.3	100	7.5	371	23.56	1	–	13.5	23.56	This work
	Wound coil	BeCu	Cu	931[c]	15k	2.3k	50	58	0.15		0.08	386.7	[16]
		Cu		1440[b]	100k		111	27	1	250	12.4[a]	27	[17]
		Si	Cu	34.5[c]	110		58.5	10.8	0.15	–	0.06	72	[10]
		Steel/BeCu	Cu	428[c]	4k	1.5k	52	46	0.15	–	0.06	306.7	[10]
		FR4	Cu	–	100	100	24.4	144	4.1	–	0.1	35.1	[29]
Moving coil	Planar coil	Parylene	Au	10	250	580	4.2–5k	0.4	1.4	1	50	0.286	[18]
		Si	Cu	–	52.7	55	9.84k	0.023	0.106	–	1	0.217	[19]
	Wound coil	Si	Cu	–	100	–	9.5k	0.122	0.1		0.4	1.22	[20]
		Steel		–	0.6		322	37	0.84	13	5.4[a]	44	[21]

[a] Calculated using equation $A = Y(2\pi F)^2$.
[b] Open circuit voltage.
[c] rms voltage.

ULV and ULP rectifier and multiplier circuit. Rectification can be achieved using ultra-low forward voltage (ULFV) diodes (example: PMEG2010AEB, NXP semiconductors, Eindhoven, Netherlands; minimum forward voltage of 30 mV for a forward current of 0.1 mA) and the voltage can be amplified up with an ULV dc–dc step-up converter (example: LTC3108, Linear Technology, Milpitas, CA, USA; operates from an input of 20 mV to provide a selectable step-up voltage outputs of 2.35, 3.3, 4.1 and 5 V).

Currently available vibration-based EMPGs are summarized in table 2. The comparison of the EMPGs is not straightforward; power density and normalized power density [2] of the devices are some criteria for the comparison. The planar coil-type EMPGs, where the number of turns ranges from 10 to 100, are no match to the EMPGs with more than 1000 turns in their wound coils. The wound coil-type EMPGs [10, 16, 17] generate relatively high voltages, mostly above 400 mV; however, the resistance of these coils is high which contributes to more power loss. Moreover, the wound coil-type EMPGs have lesser prospect in being integrated into the planar micro fabrication processes. The planar coil-type EMPGs [5, 11, 13, 14, 18, 27, 28, 30] mostly have less coil resistance but produce low output voltages (<180 mV) and will need a special ULV rectifier and multiplier circuit for practical usage.

The EMPGs [10, 12, 16, 28–30] with a natural frequency below 100 Hz perform well under base acceleration less than 2 g, and are more suitable for low level vibrations that are available in household and office environments. However, these EMPGs are not necessarily suitable for a medium and high g excitation and are prone to catastrophic failure of the spring under such conditions. The EMPGs designed for medium and high g excitations will better survive under low level of g but the generated power will be insufficient to provide meaningful amounts of power. The different EMPGs are designed for different applications such as specific vibration frequencies and amplitudes, and simply comparing their power densities might therefore not be justified.

5. Conclusions

The developed prototype vibration-based power generator was successfully tested. The device, having a volume of 1 cm^3, produced 60.1 mV open circuit voltage, 46.3 mV load voltage and 10.7 μW power when a 100 Ω resistor was connected to the EMPG at 371 Hz, base acceleration 13.5 g and base amplitude of 24.4 μm. At matching impedance it produced a maximum power of 23.56 μW corresponding to a power density of 23.56 $\mu W\ cm^{-3}$. Simulation results using an electromechanical model of the device are in good agreement with the experimental results. The power density of the harvester is comparable to other EMPGs developed using more involved fabrication processes. The current device is suitable to harvest energy for condition monitoring sensors in twin screw compressors and reciprocating engines, for example, where the vibration frequency band is from 10 to 5000 Hz at 10 to 15 g. However, the spring stiffness can be readily customized through mask design to achieve other resonant frequencies for a broader range of applications. By redesigning the parameters of the devices such as gap and the number of turns of the coil the device can be optimized in performance for other applications.

References

[1] Roundy S, Wright P K and Rabaey J M 2004 *Energy Scavenging for Wireless Sensor Networks with Special Focus on Vibrations* (Norwell, MA: Kluwer) pp 3–24

[2] Gilbert J M and Balouchi F 2008 Comparison of energy harvesting systems for wireless sensor networks *Int. J. Autom. Comput.* **05** 334–47

[3] Wowk V 2005 Machine Dynamics, Inc.: a professional machine vibration services and training firm. Article by a principal training instructor, available at http://www.machinedyn.com/revised/tutorial.pdf (cited 12 July 2010)

[4] Gao R X and Cui Y 2005 Vibration-based energy extraction for sensor powering: design, analysis, and experimental evaluation *Proc. SPIE (San Diego, CA, USA, 7 March 2005); Proc. SPIE* **5765** 794–801

[5] Khan F, Sassani F and Stoeber B 2010 Vibration-based PDMS membrane type electromagnetic power generator for low vibration environments *Proc. CSME FORUM 2010 (Victoria, Canada, 7–9 June 2010)*

[6] Anton S R and Sodano H A 2008 A review of power harvesting using piezoelectric materials (2003–2006) *Smart Mater. Struct.* **16** R1–R21

[7] Hoffmann D, Folkmer B and Manoli Y 2009 Fabrication, characterization and modelling of electrostatic micro-generators *J. Micromech. Microeng.* **19** 094001

[8] Arnold D P 2007 Review of microscale magnetic power generation *IEEE Trans. Magn.* **43** 3940–50

[9] Beeby S P, Tudor M J and White N M 2006 Energy harvesting vibration sources for microsystems applications *Meas. Sci. Technol.* **17** 175–95

[10] Beeby S P, Torah R N, Tudor M J, Glynne-Jones P, O'Donnell T, Saha C R and Roy S 2007 A micro electromagnetic generator for vibration energy harvesting *J. Micromech. Microeng.* **17** 1257–65

[11] Wang P H, Dai X H, Fang D M and Zhao X L 2007 Design, fabrication and performance of a new vibration-based electromagnetic micro power generator *Microelectron. J.* **38** 1175–80

[12] Huang W S, Tzeng K E, Cheng M C and Huang R S 2007 A silicon MEMS micro power generator for wearable micro devices *J. Chin. Inst. Eng.* **30** 133–40

[13] Pan C T, Hwang Y M, Hu H L and Liu H C 2006 Fabrication and analysis of a magnetic self-power microgenerator *J. Magn. Magn. Mater.* **304** 394–6

[14] Serre C, Peŕez-Rodrıguez A, Fondevilla N, Martincic E, Morante J R, Montserrat J and Esteve J 2009 Linear and non-linear behavior of mechanical resonators for optimized inertial electromagnetic microgenerators *Microsyst. Technol.* **15** 1217–23

[15] Wacharasindhu T and Kwon J W 2008 A micromachined energy harvester from a keyboard using combined electromagnetic and piezoelectric conversion *J. Micromech. Microeng.* **18** 104016

[16] Torah R, Glynne-Jones P, Tudor M, O'Donnell T, Roy S and Beeby S 2008 Self-powered autonomous wireless sensor node using vibration energy harvesting *Meas. Sci. Technol.* **19** 125202

[17] Yuen S C L, Lee J M H, Luk M H M, Chan G M H, Lei K F, Leong P H W, Li W J and Yam Y 2004 AA size micro power conversion cell for wireless applications *Proc. 5th World Congress on Intelligent Control and Automation (Hangzhou, China, 15–19 June 2004)* vol 6 pp 5629–34

[18] Sari I, Balkan T and Kulah H 2008 An electromagnetic micro power generator for wideband environmental vibrations *Sensors Actuators* A **145–146** 405–13

[19] Kulkarni S, Koukharenko E, Torah R, Tudor J, Beeby S, O'Donnell T and Roy S 2008 Design, fabrication and testing of integrated micro-scale vibration-based electromagnetic generator *Sensors Actuators* A **145–146** 336–42

[20] Koukharenko E, Beeby S P, Tudor M J, White N M, O'Donnell T, Saha C, Kulkarni S and Roy S 2006 Microelectromechanical systems vibration powered electromagnetic generator for wireless sensor applications *Microsyst. Technol.* **12** 1071–7

[21] Glynne-Jones P, Tudor M J, Beeby S P and White N M 2004 An electromagnetic vibration-powered generator for intelligent sensor systems *Sensors Actuators* A **110** 344–9

[22] Soliman M S M, Abdel-Rahman E M, El-Saadany E F and Mansour R R 2008 A wideband vibration-based energy harvester *J. Micromech. Microeng.* **18** 115021

[23] Sterken T, Baert K, Van Hoof C, Puers R, Borghs G and Fiorini P 2004 Comparative modelling for vibration scavengers *Proc. IEEE Sensors Conf. (Vienna, 24–27 October)* vol 3 pp 1249–52

[24] Mitcheson P D, Green T C, Yeatman E M and Holmes A S 2004 Architectures for vibration-driven micropower generators *J. Microelectromech. Syst.* **13** 429–40

[25] Svoboda J 2004 *Magnetic Techniques for the Treatment of Materials* (Dordrecht: Kluwer) pp 260–3

[26] Khan F, Sassani F and Stoeber B 2010 Vibration-based electromagnetic energy harvester *Proc. ASME IMECE2010 (Vancouver, Canada, 12–18 November 2010)*

[27] Yang B, Lee C, Xiang W, Xie J, He J H, Kotlanka R K, Low S P and Feng H 2010 Electromagnetic energy harvester from vibrations of multiple frequencies *J. Micromech. Microeng.* **19** 035001

[28] Yang B and Lee C 2010 Non-resonant electromagnetic wideband energy harvesting mechanism for low frequency vibrations *Microsyst. Technol.* **16** 961–66

[29] Hatipoglu G and Urey H 2010 FR4-based electromagnetic energy harvester for wireless sensor nodes *Smart Mater. Struct.* **19** 015022

[30] Wang P, Tanaka K, Sugiyama S, Dai X, Zhao X and Liu J 2009 A micro electromagnetic low level vibration energy harvester based on MEMS technology *Microsyst. Technol.* **15** 941–51